

# Fully charmed P-wave tetraquark resonant states in the quark model

Wei-Lin Wu<sup>1,\*</sup> and Shi-Lin Zhu<sup>2,†</sup>

<sup>1</sup>*School of Physics, Peking University, Beijing 100871, China*

<sup>2</sup>*School of Physics and Center of High Energy Physics, Peking University, Beijing 100871, China*

We conduct the first comprehensive P-wave four-body dynamical calculations of the fully charmed tetraquark systems within the quark potential model. We apply the Gaussian expansion method to solve the four-body Schrödinger equation, incorporating both dimeson and diquark-antidiquark spatial configurations. The matrix elements of P-wave states are calculated analytically using the infinitesimally-shifted Gaussian basis functions. With the complex scaling method, we obtain several fully charmed P-wave resonant states with compact tetraquark configuration in the mass region of (7.0, 7.2) GeV, including states with exotic quantum numbers  $J^{PC} = 0^{--}, 1^{-+}$ . However, we find no resonant states with the mass  $M < 7$  GeV and width  $\Gamma < 200$  MeV. Combining the present investigation with our previous results on S-wave fully charmed tetraquark systems [1], candidates for the experimental states  $X(6400)$  and  $X(6600)$  are still absent in the quark model.

## I. INTRODUCTION

As novel hadronic states beyond conventional mesons ( $q\bar{q}$ ) and baryons ( $qqq$ ), multiquark states exhibit more intricate internal structures, offering an excellent platform for studying the non-perturbative quantum chromodynamics (QCD). In the past few decades, hadron physicists have made significant progress on both the experimental and theoretical explorations of multiquark states [2–12].

The fully charmed tetraquark states serve as an ideal and relatively pure multiquark system. Without the light degrees of freedom, it is unaffected by the complicated coupled-channel effects between the tetraquark states and  $c\bar{c}$  mesons, as in the case of  $X(3872)$ . Moreover, the long-range light meson exchange mechanism is absent, making compact tetraquark states arising from short-range gluon exchange interactions more likely to exist. Several experimental candidates of the fully charmed tetraquark states have been reported in the  $J/\psi J/\psi$  and  $J/\psi\psi(2S)$  decay channels. Specifically,  $X(6900)$  was first discovered by the LHCb Collaboration [13] and later confirmed by the CMS [14] and ATLAS [15].  $X(6400)$  was reported by the ATLAS [15], while  $X(6600)$  and  $X(7200)$  were reported by both the CMS [14] and ATLAS [15]. Numerous theoretical studies have discussed the experimentally observed fully charmed tetraquark states, offering various interpretations within different frameworks [16–58]. In our previous work [1], we carried out benchmark calculations of the S-wave fully charmed tetraquark systems within the quark potential model. We obtained compact tetraquark candidates for  $X(6900)$  and  $X(7200)$  in the  $J^{PC} = 0^{++}$  and  $2^{++}$  systems, but found no signals for  $X(6400)$  and  $X(6600)$ .

It is natural to wonder whether parity negative P-wave fully charmed tetraquark states exist or not. Compared to the S-wave systems, P-wave tetraquark systems may contain more complex correlations among color, spin, and spatial degrees of freedom, due to the presence of various excitation modes and the inclusion of spin-orbit and tensor potentials. Investi-

gations of the P-wave systems may enhance our understanding of exotic hadrons and enrich the hadron spectrum. The P-wave fully charmed tetraquark system was studied in the the QCD sum rule [20, 43, 59, 60], coupled-channels formalism [54], diquark-antidiquark model [22, 61, 62], and the quark model with diquark-antidiquark configuration [16, 17, 41, 53]. However, the diquark-antidiquark picture does not consider the channel coupling effects with meson-meson continuum states and may lead to the misidentification of resonant states.

In this work, we conduct the first comprehensive P-wave four-body dynamical calculations of the fully charmed tetraquark systems within the quark potential model. We employ the Gaussian expansion method [63] and incorporate both dimeson and diquark-antidiquark spatial configurations to solve the four-body Schrödinger equation. The matrix elements of P-wave states are calculated analytically using the infinitesimally-shifted Gaussian basis functions. We utilize the complex scaling method [64–66] to distinguish genuine resonant states from meson-meson continuum states. We analyze the spatial structures of the resonant states by calculating their root-mean-square radii, which can clearly reveal whether they are meson molecules or compact tetraquark states. This framework has been successfully used to investigate S-wave tetraquark bound and resonant states [1, 67–70].

This paper is organized as follows. In Sec. II, we introduce the theoretical framework, including the quark potential model, the wave function construction, the complex scaling method and the analysis of spatial structures. In Sec. III, we present the numerical results and discussions. We summarize our findings in Sec. IV.

## II. THEORETICAL FRAMEWORK

### A. Hamiltonian

We employ the nonrelativistic quark potential model proposed in Ref. [71] to study the fully charmed tetraquark sys-

\* wlwu@pku.edu.cn

† zhushi@pku.edu.cn

tems. The Hamiltonian in the center-of-mass frame reads

$$H = \sum_{i=1}^4 (m_i + \frac{p_i^2}{2m_i}) + \sum_{i<j=1}^4 V_{ij}, \quad (1)$$

with  $m_i$  and  $p_i$  being the mass and momentum of the (anti)quark  $i$ . The two-body potential  $V_{ij}$ , which results from the one-gluon-exchange and linear confinement interactions, consists of the central potential  $V_{\text{cen}}$ , spin-orbit potential  $V_{\text{so}}$ , and tensor potential  $V_{\text{ts}}$ ,

$$\begin{aligned} V_{ij} &= -\frac{3}{16} \boldsymbol{\lambda}_i \cdot \boldsymbol{\lambda}_j (V_{\text{cen}}(r_{ij}) + V_{\text{so}}(r_{ij}) + V_{\text{ts}}(r_{ij})), \\ V_{\text{cen}}(r_{ij}) &= -\frac{4}{3} \frac{\alpha_s}{r_{ij}} + br_{ij} + \frac{32\pi\alpha_s}{9m_c^2} \delta^{(3)}(\mathbf{r}_{ij}) \mathbf{S}_i \cdot \mathbf{S}_j, \\ V_{\text{so}}(r_{ij}) &= \frac{1}{m_c^2} \left( \frac{2\alpha_s}{r_{ij}^3} - \frac{b}{2r_{ij}} \right) \mathbf{L}_{ij} \cdot (\mathbf{S}_i + \mathbf{S}_j), \\ V_{\text{ts}}(r_{ij}) &= \frac{4\alpha_s}{3m_c^2} \frac{1}{r_{ij}^3} \left( \frac{3(\mathbf{S}_i \cdot \mathbf{r}_{ij})(\mathbf{S}_j \cdot \mathbf{r}_{ij})}{r_{ij}^2} - \mathbf{S}_i \cdot \mathbf{S}_j \right), \end{aligned} \quad (2)$$

where  $\boldsymbol{\lambda}_i$  and  $\mathbf{S}_i$  are the SU(3) color Gell-Mann matrix and the spin operator acting on (anti)quark  $i$ , respectively.  $r_{ij}$  is the distance between (anti)quark  $i$  and  $j$ , and  $\mathbf{L}_{ij}$  is the relative orbital angular momentum operator.

In the Schrödinger equation, the  $\delta^{(3)}(\mathbf{r})$  and  $\frac{1}{r^3}$  terms have singularities, which are artifacts of the nonrelativistic approximation. To avoid the singularities, the former is regularized by a Gaussian smearing function,

$$\delta^{(3)}(\mathbf{r}) \rightarrow \frac{\sigma^3 \exp(-\sigma^2 r^2)}{\pi^{3/2}}, \quad (3)$$

while the  $\frac{1}{r^3}$  terms in  $V_{\text{so}}$  and  $V_{\text{ts}}$  are often treated as perturbations in literature [41, 71]. In this work we treat both singular terms in a consistent way by regularizing the  $\frac{1}{r^3}$  terms as follows,

$$\frac{1}{r^3} \rightarrow \frac{(1 - e^{-\sigma_1^2 r^2})^2}{r^3}. \quad (4)$$

Instead of treating  $V_{\text{so}}$  and  $V_{\text{ts}}$  as perturbations, we solve the Schrödinger equation by diagonalizing the complete Hamiltonian with the regularized potential. The parameters for the potential are listed in Table I. The first four parameters, which are taken from Ref. [71], were determined by fitting the charmonium spectrum. The last parameter  $\sigma_1$  is determined by fitting the  $\chi_{cJ}$  spectrum. Both the parameters  $\sigma$  and  $\sigma_1$  are comparable to  $m_c$ , which are reasonable for regularization to the nonrelativistic approximation. The theoretical masses of the charmonia as well as their root-mean-square (rms) radii are listed in Table II. Both the results from the regularized potential and the perturbation method are consistent with the experimental values within tens of MeV. Accordingly, we expect the uncertainties of the tetraquark spectrum to be of the same order.

TABLE I. The parameters in the potential.

$\alpha_s$	$b[\text{GeV}^2]$	$m_c[\text{GeV}]$	$\sigma[\text{GeV}]$	$\sigma_1[\text{GeV}]$
0.5461	0.1425	1.4794	1.0946	1.3133

TABLE II. The theoretical masses  $m_{\text{Theo.}}$  (in MeV) of charmonia using the regularized potential, compared with the experimental results  $m_{\text{Exp.}}$  taken from Ref. [72], and the theoretical results  $m_{\text{Per.}}$  in Ref. [71] using the perturbation method. The rms radii (in fm) are listed in the last column.

Mesons	$m_{\text{Exp.}}$	$m_{\text{Theo.}}$	$m_{\text{Per.}}$	$r_{\text{Theo.}}^{\text{rms}}$
$\eta_c$	2984	2982	2982	0.36
$\eta_c(2S)$	3638	3630	3630	0.83
$J/\psi$	3097	3090	3090	0.41
$\psi(2S)$	3686	3672	3672	0.86
$\psi(3S)$	4040	4072	4072	1.24
$\chi_{c0}$	3415	3426	3424	0.59
$\chi_{c1}$	3511	3511	3505	0.67
$\chi_{c2}$	3556	3544	3556	0.71
$h_c$	3525	3516	3516	0.67
$\chi_{c0}(2P)$	...	3876	3852	1.01
$\chi_{c1}(2P)$	...	3933	3925	1.07
$\chi_{c2}(2P)$	...	3959	3972	1.10
$h_c(2P)$	...	3934	3934	1.07

## B. Wave function

The P-wave tetraquark wave functions are expanded using a set of basis functions, which are written as

$$\psi^J = \mathcal{A}(\chi^S \otimes \Phi^{L=1})^J, \quad (5)$$

where  $\mathcal{A}$  is the antisymmetric operator of identical particles,  $\phi^{L=1}$  and  $\chi^S$  represent the P-wave spatial wave function and color-spin wave function with total spin  $S$ , respectively. The total angular momentum  $J = L \oplus S$ . A complete set of the color-spin wave function is used,

$$\begin{aligned} \chi_{\bar{3}_c \otimes \bar{3}_c}^{S, s_1, s_2} &= [(Q_1 Q_2)_{\bar{3}_c}^{s_1} (\bar{q}_1 \bar{q}_2)_{\bar{3}_c}^{s_2}]_{1_c}^S, \\ \chi_{6_c \otimes \bar{6}_c}^{S, s_1, s_2} &= [(Q_1 Q_2)_{6_c}^{s_1} (\bar{q}_1 \bar{q}_2)_{\bar{6}_c}^{s_2}]_{1_c}^S, \end{aligned} \quad (6)$$

for all possible combinations of  $S, s_1, s_2$ . The subscripts and superscripts denote the color and spin representations, respectively.

For the spatial wave function, we employ the Gaussian expansion method [63] and consider three sets of spatial configurations (dimeson and diquark-antidiquark), which are denoted by (jac) = (a), (b), (c). In each configuration, there are three independent Jacobian coordinates  $\rho_1, \rho_2, \lambda$ , as shown in Fig. 1. We consider one orbital excitation, i.e., the  $\rho$  mode excitation  $|l_{\rho_1} = 1, l_{\rho_2} = l_\lambda = 0\rangle$  or  $|l_{\rho_1} = 0, l_{\rho_2} = 1, l_\lambda = 0\rangle$ , and the  $\lambda$  mode excitation  $|l_{\rho_1} = l_{\rho_2} = 0, l_\lambda = 1\rangle$ . The spatial basis functions are written as

$$\Phi_{n_1, n_2, n_3}^{L=1} = \phi_{n_1 l_{\rho_1}}(\rho_1) \phi_{n_2 l_{\rho_2}}(\rho_2) \phi_{n_3 l_{\lambda}}(\lambda) \cdot \left[ (Y_{l_{\rho_1}}(\hat{\rho}_1) \otimes Y_{l_{\rho_2}}(\hat{\rho}_2)) \otimes Y_{l_{\lambda}}(\hat{\lambda}) \right]^{L=1}. \quad (7)$$

$\phi_{nl}(r)$  takes the Gaussian form,

$$\phi_{nl}(r) = N_{nl} r^l e^{-\nu_n r^2}, \quad (8)$$

$$\nu_n = \nu_1 \gamma^{n-1} \quad (n = 1 \sim n_{\max}),$$

where  $N_{nl}$  is the normalization factor. To obtain numerically stable results, we take  $n_{\max} = 10 \sim 12$ , and the total number of bases is  $10^4 \sim 10^5$ .

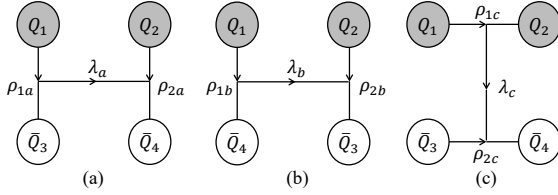


FIG. 1. The Jacobian coordinates for two types of spatial configurations: (a), (b) for the meson configurations, and (c) for the diquark-antidiquark configuration.

To evaluate the spatial matrix elements of P-wave states, we make use of the infinitesimally-shifted Gaussian basis functions [63], which circumvent the need for carrying out complicated integrals of spherical harmonics of different configurations. We present the details in Appendix A.

### C. Complex scaling method

The wave functions of resonant states are not square integrable, causing challenges for solving the Schrödinger equation numerically. To obtain possible bound states and resonant states, we employ the complex scaling method (CSM) [64–66], where the coordinate  $\mathbf{r}$  and its conjugate momentum  $\mathbf{p}$  are transformed as

$$U(\theta)\mathbf{r} = \mathbf{r}e^{i\theta}, \quad U(\theta)\mathbf{p} = \mathbf{p}e^{-i\theta}. \quad (9)$$

Under such a transformation, the Hamiltonian is analytically continued to the complex energy plane and no longer Hermitian,

$$H(\theta) = \sum_{i=1}^4 \left( m_i + \frac{p_i^2 e^{-2i\theta}}{2m_i} \right) + \sum_{i<j=1}^4 V_{ij}(\mathbf{r}_{ij} e^{i\theta}). \quad (10)$$

The asymptotic behavior of the wave functions is also modified. If the complex scaling angle  $\theta \in [0, \frac{\pi}{2})$ , the wave functions of bound states remain square integrable. They are located on the negative real axis in the energy plane. If  $\theta > \theta_r = \frac{1}{2} \tan^{-1}(\Gamma_r/2M_r)$ , where  $M_r$  and  $\Gamma_r$  represent its mass and width, the wave functions of the resonant states become square integrable and are obtained with eigenenergy

$E_r = M_r - i\Gamma_r/2$ . Scattering states align along rays starting from threshold energies with  $\text{Arg}(E) = -2\theta$ . By choosing appropriate complex scaling angles and solving the complex scaled Schrödinger equation, we can obtain bound states, resonant states and scattering states simultaneously.

### D. Spatial structures

Generally, tetraquark states are classified into meson molecules and compact tetraquarks. Both configurations are allowed in the quark model, where no assumptions regarding the clustering of quarks are made. In our previous works [1, 68], we have proposed to use the rms radii to analyze the spatial structures of tetraquark states. We decompose the complete antisymmetric wave function as

$$\begin{aligned} \Psi(\theta) &= \sum_{S, s_1 \geq s_2} \left( [(Q_1 \bar{Q}_3)_{1_c}^{s_1} (Q_2 \bar{Q}_4)_{1_c}^{s_2}]^S \otimes |\psi_1^{S, s_1 s_2}(\theta)\rangle \right. \\ &\quad + [(Q_1 \bar{Q}_3)_{1_c}^{s_2} (Q_2 \bar{Q}_4)_{1_c}^{s_1}]^S \otimes |\psi_2^{S, s_1 s_2}(\theta)\rangle \\ &\quad + [(Q_1 \bar{Q}_4)_{1_c}^{s_1} (Q_2 \bar{Q}_3)_{1_c}^{s_2}]^S \otimes |\psi_3^{S, s_1 s_2}(\theta)\rangle \\ &\quad \left. + [(Q_1 \bar{Q}_4)_{1_c}^{s_2} (Q_2 \bar{Q}_3)_{1_c}^{s_1}]^S \otimes |\psi_4^{S, s_1 s_2}(\theta)\rangle \right) \\ &= \mathcal{A} \sum_{S, s_1 \geq s_2} [(Q_1 \bar{Q}_3)_{1_c}^{s_1} (Q_2 \bar{Q}_4)_{1_c}^{s_2}]^S \otimes |\psi_1^{S, s_1 s_2}(\theta)\rangle \\ &\equiv \mathcal{A} \Psi_{\text{nA}}(\theta), \end{aligned} \quad (11)$$

Instead of using the complete wave function  $\Psi(\theta)$ , we use the decomposed non-antisymmetric wave function  $\Psi_{\text{nA}}(\theta)$  to calculate the rms radius:

$$r_{ij}^{\text{rms}} \equiv \text{Re} \left[ \sqrt{\frac{\langle \Psi_{\text{nA}}(\theta) | r_{ij}^2 e^{2i\theta} | \Psi_{\text{nA}}(\theta) \rangle}{\langle \Psi_{\text{nA}}(\theta) | \Psi_{\text{nA}}(\theta) \rangle}} \right]. \quad (12)$$

This definition of the rms radius has been successfully used to distinguish between meson molecules and compact tetraquarks in various systems [1, 68–70, 73]. For a meson molecule,  $Q_1 \bar{Q}_3$  and  $Q_2 \bar{Q}_4$  form two color singlets in  $\Psi_{\text{nA}}(\theta)$ , so  $r_{13}^{\text{rms}}$  and  $r_{24}^{\text{rms}}$  are expected to be the sizes of the constituent mesons, and much smaller than the other rms radii. For a compact tetraquark state, all four (anti)quarks are confined together, and all rms radii are on the order of  $\Lambda_{QCD}^{-1} \sim 1$  fm. It is worth noting that the rms radii obtained from the conventional definition using the complete wave function  $\Psi(\theta)$  and those from our novel definition are qualitatively consistent for compact tetraquarks, as discussed in Refs. [1, 70].

## III. RESULTS AND DISCUSSIONS

We investigate the P-wave fully charmed tetraquark systems with all possible quantum numbers, including  $J^{PC} = 0^{-+}, 0^{--}, 1^{-+}, 1^{--}, 2^{-+}, 2^{--}, 3^{-+}, 3^{--}$ . We choose varying complex scaling angles  $\theta$  in the CSM to calculate the complex energy spectra. The results for C-parity positive and negative systems are shown in Figs. 2 and 3, respectively. All

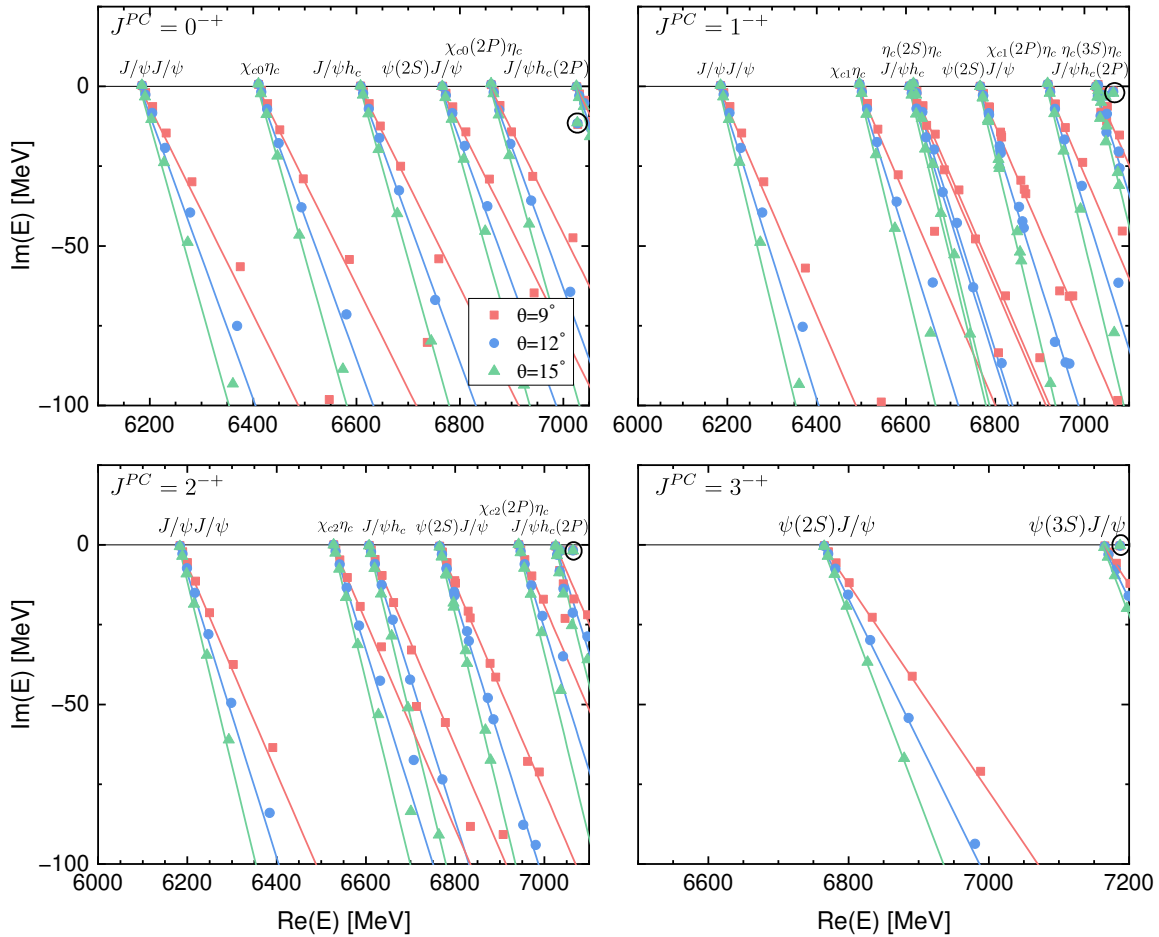


FIG. 2. The complex energy eigenvalues of C-parity positive  $c\bar{c}\bar{c}\bar{c}$  states with varying  $\theta$  in the CSM. The solid lines represent the continuum lines rotating along  $\text{Arg}(E) = -2\theta$ . The resonances do not shift as  $\theta$  changes and are highlighted by the circles.

of the states lie above the lowest dimeson threshold and no P-wave tetraquark bound state is found. We obtain meson-meson scattering states of all possible channels and several resonant states, which are labeled as  $T_{4c,J^{PC}}(M)$  with  $M$  being the mass of the state. The resonant states are found in the mass region of (7.0, 7.2) GeV. They are located near the  $M(1S)M'(2P)$  thresholds, except in the  $3^{-+}$  system where no such dimeson threshold exists, and  $T_{4c,3^{-+}}(7187)$  lies above the  $\psi(3S)J/\psi$  threshold. In the  $1^{--}$  system, resonant states above 7 GeV might exist, but we fail to identify them since the dimeson thresholds in the region are nearly degenerate, making it very difficult to identify resonant states from continuum states unambiguously in the current calculations.

The complex energies, proportions of different color and spin configurations and rms radii of the resonant states are summarized in Table III. The resonant states are mixtures of  $\chi_{\bar{3}_c \otimes 3_c}$  and  $\chi_{6_c \otimes \bar{6}_c}$  configurations, suggesting that the color configuration mixing effect plays an important role. On the contrary, the mixing effect between different spin configurations is small, and the resonant state is dominated by one single  $\chi^S$  component. This is expected since the spin mixing effect can only be induced by spin-orbit and tensor potentials, which are high-order corrections with small contributions.

The rms radii of the resonant states are on the order of  $\Lambda_{QCD}^{-1} \sim 1$  fm, indicating that they are all compact tetraquark states. Based on the classifications of compact tetraquarks proposed in Ref. [70],  $T_{4c,0^{-+}}(7028)$  is a compact diquark-antidiquark tetraquark, as its rms radii  $r_{c_1 c_2}^{\text{rms}}$ ,  $r_{\bar{c}_3 \bar{c}_4}^{\text{rms}}$  are relatively small. The other resonant states are compact even tetraquarks, where the relative distances between four (anti)quarks are of similar size. The rms radii for  $T_{4c,2^{--}}(7025)$  changes drastically as  $\theta$  varies, which may result from the fact that the state lies very close to the dimeson threshold and is strongly coupled to the scattering states. We cannot obtain numerically stable results and determine its configuration in the current calculation.

The resonant states have various decay channels, as shown in Figs. 2 and 3. Their S-wave and P-wave strong decay modes are summarized in Table IV. Among these states,  $T_{4c,0^{--}}(7080)$  and  $T_{4c,1^{-+}}(7065)$  are of particular interest. They have exotic quantum numbers which are not accessible by  $c\bar{c}$  mesons. The former can be searched for in the S-wave  $J/\psi\chi_{c1}$  and P-wave  $J/\psi\eta_c$  channels, while the latter can be searched for in the S-wave  $\chi_{c1}\eta_c$ ,  $J/\psi h_c$ , and P-wave  $J/\psi J/\psi$  channels.  $T_{4c,3^{-+}}(7187)$  has the smallest width 0.6 MeV, which may be due to the fact that it has no S-wave decay

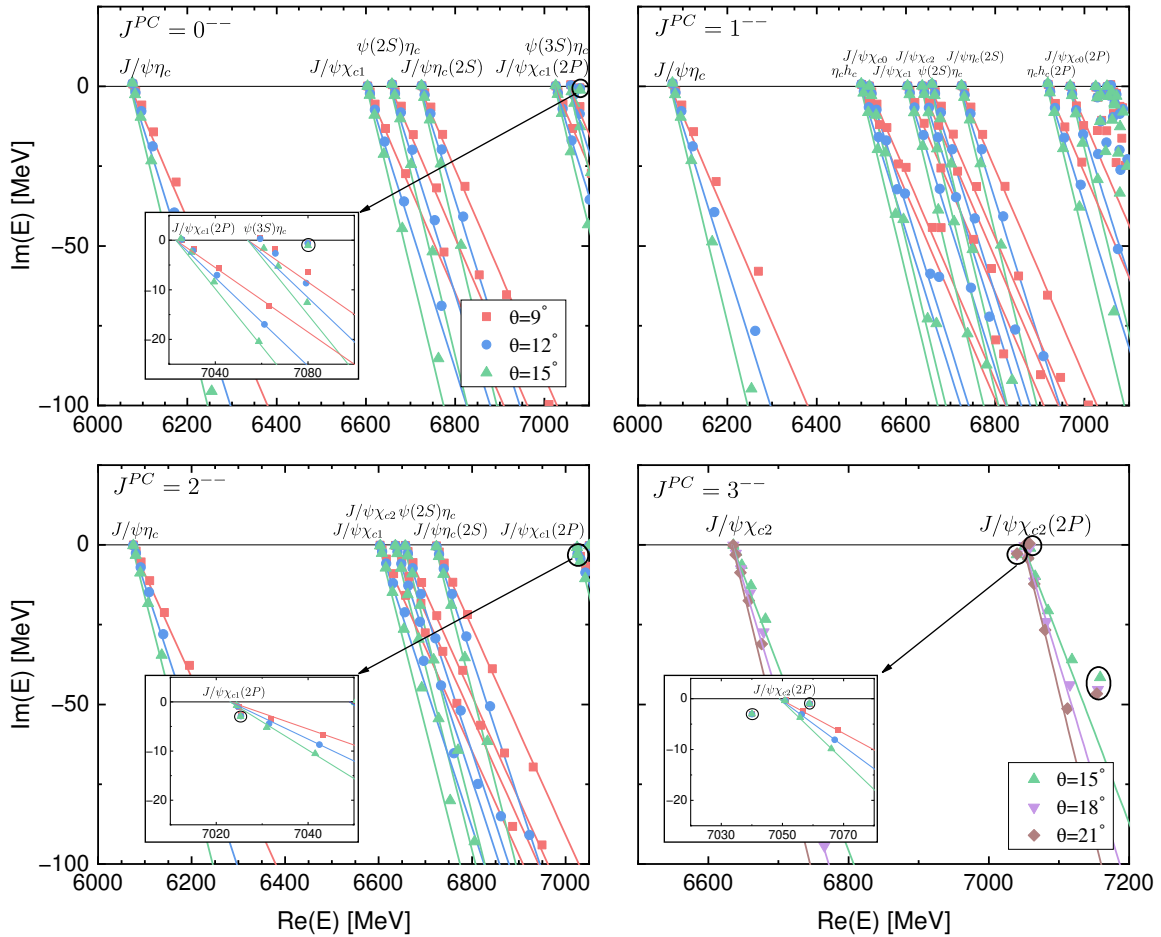


FIG. 3. The complex energy eigenvalues of C-parity negative  $cc\bar{c}\bar{c}$  states with varying  $\theta$  in the CSM. The solid lines represent the continuum lines rotating along  $\text{Arg}(E) = -\theta$ . The resonances do not shift as  $\theta$  changes and are highlighted by the circles.

TABLE III. The complex energies (in MeV), proportions of different color and spin configurations and rms radii (in fm) of the  $cc\bar{c}\bar{c}$  resonant states. The “?” indicates that the rms radii results are numerically unstable as the complex scaling angle  $\theta$  varies.

$J^{PC}$	$M - i\Gamma/2$	$\chi_{\text{color}}$		$\chi^{\text{spin}}$			$r^{\text{rms}}$			
		$\chi_{\bar{3}_c \otimes 3_c}$	$\chi_{6_c \otimes \bar{6}_c}$	$\chi^{S=0}$	$\chi^{S=1}$	$\chi^{S=2}$	$r_{c_1 \bar{c}_3}^{\text{rms}}$	$r_{c_2 \bar{c}_4}^{\text{rms}}$	$r_{c_1 \bar{c}_4}^{\text{rms}} = r_{c_2 \bar{c}_3}^{\text{rms}}$	$r_{c_1 \bar{c}_2}^{\text{rms}} = r_{c_3 \bar{c}_4}^{\text{rms}}$
$0^{-+}$	$7028 - 12i$	68%	32%	-	100%	-	0.75	0.96	0.69	0.47
$0^{-}$	$7080 - 1i$	20%	80%	-	100%	-	0.74	0.73	0.84	0.95
$1^{-+}$	$7065 - 2i$	24%	76%	0%	100%	0%	0.66	0.77	0.88	0.94
$2^{-+}$	$7064 - 2i$	27%	73%	-	100%	0%	0.67	0.78	0.84	0.86
$2^{-}$	$7025 - 3i$	73%	27%	-	5%	95%	0.87	0.87	?	?
$3^{-+}$	$7187 - 0.3i$	85%	15%	-	-	100%	0.82	0.82	0.84	0.79
$3^{-}$	$7040 - 3i$	77%	23%	-	-	100%	0.89	0.89	1.04	0.85
	$7059 - 1i$	45%	55%	-	-	100%	0.75	0.75	1.00	0.86
	$7154 - 46i$	72%	28%	-	-	100%	0.95	0.95	1.03	0.95

mode and can only decay into the  $\psi(2S)J/\psi$  and  $\psi(3S)J/\psi$  channels via P-wave transitions. It should be noted that the theoretical widths of the tetraquark resonant states are underestimated, since the widths of charmonia are not taken into account. Moreover, other decay modes via the annihilation of charmed quarks are also not considered in the quark model.

Combining our previous work on S-wave fully charmed tetraquark system [1], we find that the lowest resonant state in both S-wave and P-wave systems are located around 7 GeV. In S-wave systems, good candidates for  $X(6900)$  and  $X(7200)$  are obtained in the  $J^{PC} = 0^{++}$  and  $2^{++}$  systems. Their masses and widths are comparable with the experimental re-

TABLE IV. The S-wave and P-wave two-body strong decay modes of the  $cc\bar{c}\bar{c}$  resonant states.

States	S-wave	P-wave
$T_{4c,0-+}$ (7028)	$\chi_{c0}\eta_c, J/\psi h_c, \chi_{c0}(2P)\eta_c, J/\psi h_c(2P)$	$J/\psi J/\psi, \psi(2S)J/\psi$
$T_{4c,0--}$ (7080)	$J/\psi\chi_{c1}, J/\psi\chi_{c1}(2P)$	$J/\psi\eta_c, \psi(2S)\eta_c, J/\psi\eta_c(2S), \eta_c\psi(3S)$
$T_{4c,1-+}$ (7065)	$\chi_{c1}\eta_c, J/\psi h_c, \chi_{c1}(2P)\eta_c, J/\psi h_c(2P)$	$J/\psi J/\psi, \eta_c(2S)\eta_c, \psi(2S)J/\psi, \eta_c(3S)\eta_c$
$T_{4c,2-+}$ (7064)	$\chi_{c2}\eta_c, J/\psi h_c, \chi_{c2}(2P)\eta_c, J/\psi h_c(2P)$	$J/\psi J/\psi, \psi(2S)J/\psi$
$T_{4c,2--}$ (7025)	$J/\psi\chi_{c1}, J/\psi\chi_{c2}, J/\psi\chi_{c1}(2P)$	$J/\psi\eta_c, \psi(2S)\eta_c, J/\psi\eta_c(2S)$
$T_{4c,3-+}$ (7187)	-	$\psi(2S)J/\psi, \psi(3S)J/\psi$
$T_{4c,3--}$ (7040)	$J/\psi\chi_{c2}$	-
$T_{4c,3--}$ (7059)	$J/\psi\chi_{c2}, J/\psi\chi_{c2}(2P)$	-
$T_{4c,3--}$ (7154)	$J/\psi\chi_{c2}, J/\psi\chi_{c2}(2P)$	-

sults. However, the widths of the P-wave resonant states that can decay into the  $J/\psi J/\psi$  or  $J/\psi\psi(2S)$  channels are significantly smaller than the experimental widths of  $X(6900)$  and  $X(7200)$ , which are around 100 MeV [13–15]. Therefore, these narrow P-wave resonances remain to be discovered experimentally. They might be hidden within the broad structures of S-wave states in the  $J/\psi J/\psi$  or  $J/\psi\psi(2S)$  decay channels.

The broad structure ranging from 6.2 to 6.8 GeV in the experiments remains elusive and unseen in the quark model calculations. One possible explanation could be that the structure arises from extremely broad states. In this work and our previous work on S-wave systems [1], we only focus on states with widths  $\Gamma < 200$  MeV. The wave functions of states with larger widths are more divergent, and larger complex scaling angles are needed for numerically stable results, which are difficult to achieve with the current level of precision. Therefore, if  $X(6400)$  and  $X(6600)$  are states with widths larger than 200 MeV, as suggested by the experimental results [14, 15], they cannot be obtained numerically in the current calculations. Other possibilities include modifications of confinement mechanism in the quark model [55], or contributions from dynamical effects rather than tetraquark resonant poles [23].

#### IV. SUMMARY

We calculate the energy spectrum of P-wave fully charmed tetraquark systems within the quark potential model. The two-body potential consists of the central term, spin-orbit term and tensor term, which arise from the one-gluon-exchange and linear confinement interactions. We diagonalize the complete Hamiltonian instead of treating the spin-orbit and tensor terms as perturbations. We solve the four-body Schrödinger equation using the Gaussian expansion method, taking both meson and diquark-antidiquark spatial configurations into account. We employ the complex scaling method to distinguish tetraquark resonant states from meson-meson scattering states.

We obtain fully charmed P-wave tetraquark resonant states in the mass region of (7.0, 7.2) GeV. From the root-mean-square radii, we find that they all have compact tetraquark

configurations, which are consistent with our previous findings in S-wave fully heavy tetraquark systems [1, 69]. The color mixing effect between  $\chi_{\bar{3}_c\otimes 3_c}$  and  $\chi_{6_c\otimes \bar{6}_c}$  configurations plays a vital role in the resonant states, while the mixing between different spin configurations  $\chi^S$  is very weak. Tetraquark resonant states with exotic quantum numbers  $J^{PC} = 0^{--}$  and  $1^{-+}$  lie around 7.1 GeV. They can be searched for in future experiments.

We have obtained good candidates for experimentally observed  $X(6900)$  and  $X(7200)$  in S-wave fully charmed tetraquark systems [1]. Most of the P-wave fully charmed resonances are rather narrow and do not match well with experimentally observed states. These states await experimental discoveries in the near future. The broad structure ranging from 6.2 to 6.8 GeV in the experiments remains absent in both S-wave and P-wave systems in the quark model calculations. If the structure arises from resonant states with widths larger than 200 MeV, they cannot be obtained numerically in the current calculations. Further theoretical studies and experimental measurements are needed to understand  $X(6400)$  and  $X(6600)$  better.

#### ACKNOWLEDGMENTS

We thank Dr. Lu Meng, Yan-Ke Chen, Dr. Yao Ma, Dr. Jun-Zhang Wang and Liang-Zhen Wen for the helpful discussions. This project was supported by the National Natural Science Foundation of China (No. 12475137). The computational resources were supported by High-performance Computing Platform of Peking University.

## Appendix A: Matrix element

Direct evaluation of the spatial matrix elements of P-wave states involves complicated integrals of spherical harmonics of different configurations. To avoid this, we make use of the infinitesimally-shifted Gaussian basis functions [63]. The P-wave Gaussian basis can be expressed as

$$r e^{-\nu r^2} Y_{1m}(\hat{r}) = \mathbf{k} \cdot \mathbf{r} e^{-\nu r^2} = \lim_{\epsilon_a, \epsilon_b \rightarrow 0} \frac{1}{4\epsilon_a \epsilon_b} [e^{-\nu(r-\epsilon_a \mathbf{k})^2} - e^{-\nu(r+\epsilon_b \mathbf{k})^2}], \quad (\text{A1})$$

with

$$\mathbf{k} = \begin{cases} \left( -\sqrt{\frac{3\pi}{8}}, -\sqrt{\frac{3\pi}{8}}i, 0 \right), & m = 1 \\ \left( 0, 0, \sqrt{\frac{3\pi}{4}} \right), & m = 0 \\ \left( \sqrt{\frac{3\pi}{8}}, -\sqrt{\frac{3\pi}{8}}i, 0 \right), & m = -1 \end{cases}. \quad (\text{A2})$$

To evaluate matrix elements of the central potential, we need to carry out the following type of integrals,

$$\lim_{\epsilon_a, \epsilon_b \rightarrow 0} \frac{1}{\epsilon_a \epsilon_b} \int d\mathcal{R}_c e^{-(\mathcal{R}_a^T - \mathcal{K}_a^T \epsilon_a) \nu_a (\mathcal{R}_a - \epsilon_a \mathcal{K}_a)} f(r_{c3}) e^{-(\mathcal{R}_b^T - \mathcal{K}_b^T \epsilon_b) \nu_b (\mathcal{R}_b - \epsilon_b \mathcal{K}_b)}, \quad (\text{A3})$$

with  $\mathcal{R}_\alpha = (r_{\alpha 1}, r_{\alpha 2}, r_{\alpha 3})$  being a set of Jacobian coordinates. By carrying out the transformation  $\mathcal{R}_a = U_{ac} \mathcal{R}_c$ ,  $\mathcal{R}_b = U_{bc} \mathcal{R}_c$ , the integral can be expressed as

$$\begin{aligned} & \int d\mathcal{R}_c e^{-(\mathcal{R}_c^T - \mathcal{D}^T) \mathcal{A} (\mathcal{R}_c - \mathcal{D}) - \mathcal{C}} f(r_{c3}) \\ &= \int d\mathcal{R}_c e^{-(\mathcal{R}_c^T - \mathcal{D}^T) \mathcal{B}^T \mathcal{B} (\mathcal{R}_c - \mathcal{D}) - \mathcal{C}} f(r_{c3}) \\ &= \det(\mathcal{B}^{-1})^3 \int d\tilde{\mathcal{R}}_c e^{-(\tilde{\mathcal{R}}_c - \tilde{\mathcal{D}})^2 - \mathcal{C}} f(\mathcal{B}_{33}^{-1} \tilde{r}_{c3}), \end{aligned} \quad (\text{A4})$$

where  $\mathcal{A}$  is a real symmetric matrix. In the second line, the Cholesky decomposition  $\mathcal{A} = \mathcal{B}^T \mathcal{B}$  is used, with  $\mathcal{B}$  being an upper triangular matrix. In the last line,  $\mathcal{R}_c, \mathcal{D}$  are transformed as  $\tilde{\mathcal{R}}_c = \mathcal{B} \mathcal{R}_c, \tilde{\mathcal{D}} = \mathcal{B} \mathcal{D}$ . The Gaussian integral (A4) can be carried out analytically, which are kept up to terms linear in  $\epsilon_a \epsilon_b$  to give the final results of Eq. (A3).

The spatial part of the tensor potential takes the form,

$$V_{ts} \sim \frac{r_i r_j}{r^5}, \quad (\text{A5})$$

while for the spin-orbit potential, the orbital angular momentum operator is written as

$$L_i = \epsilon_{ijk} r_j p_k = -i \epsilon_{ijk} r_j \frac{\partial}{\partial r_k}. \quad (\text{A6})$$

The derivative acts on the Gaussian basis to give a constant or  $r_k$  factor. Therefore, we need to carry out the integrals of the form,

$$\begin{aligned} & \int d\tilde{\mathcal{R}}_c e^{-(\tilde{\mathcal{R}}_c - \tilde{\mathcal{D}})^2 - \mathcal{C}} f(\tilde{r}_{c3}) \tilde{r}_{c3,j}, \\ & \int d\tilde{\mathcal{R}}_c e^{-(\tilde{\mathcal{R}}_c - \tilde{\mathcal{D}})^2 - \mathcal{C}} f(\tilde{r}_{c3}) \tilde{r}_{c3,j} \tilde{r}_{c3,k}, \end{aligned} \quad (\text{A7})$$

where  $\tilde{r}_{c3,i}$  denotes the  $i$ -th component of the coordinate  $\tilde{\mathbf{r}}_{c3}$ . The integrals in Eq. (A7) can be related to the integral in Eq. (A4) by taking derivatives with respect to  $\tilde{\mathcal{D}}_{3,j}$  and  $\tilde{\mathcal{D}}_{3,k}$ ,

$$\begin{aligned} & \int d^3 r f(r) e^{-(r-d)^2} r_j = e^{-d^2} \frac{\partial}{2\partial d_j} \int d^3 r f(r) e^{-r^2 + 2\mathbf{d} \cdot \mathbf{r}}, \\ & \int d^3 r f(r) e^{-(r-d)^2} r_j r_k = e^{-d^2} \frac{\partial}{2\partial d_j} \frac{\partial}{2\partial d_k} \int d^3 r f(r) e^{-r^2 + 2\mathbf{d} \cdot \mathbf{r}}. \end{aligned} \quad (\text{A8})$$

Using the analytical solutions of Eq. (A4), the integrals in Eq. (A7) can also be carried out analytically.

- 
- [1] W.-L. Wu, Y.-K. Chen, L. Meng, and S.-L. Zhu, Benchmark calculations of fully heavy compact and molecular tetraquark states, *Phys. Rev. D* **109**, 054034 (2024), arXiv:2401.14899 [hep-ph].
- [2] H.-X. Chen, W. Chen, X. Liu, and S.-L. Zhu, The hidden-charm pentaquark and tetraquark states, *Phys. Rept.* **639**, 1 (2016), arXiv:1601.02092 [hep-ph].
- [3] A. Esposito, A. Pilloni, and A. D. Polosa, Multiquark Resonances, *Phys. Rept.* **668**, 1 (2017), arXiv:1611.07920 [hep-ph].
- [4] A. Hosaka, T. Iijima, K. Miyabayashi, Y. Sakai, and S. Yasui, Exotic hadrons with heavy flavors: X, Y, Z, and related states,

*PTEP* **2016**, 062C01 (2016), arXiv:1603.09229 [hep-ph].

- [5] R. F. Lebed, R. E. Mitchell, and E. S. Swanson, Heavy-Quark QCD Exotica, *Prog. Part. Nucl. Phys.* **93**, 143 (2017), arXiv:1610.04528 [hep-ph].
- [6] F.-K. Guo, C. Hanhart, U.-G. Meißner, Q. Wang, Q. Zhao, and B.-S. Zou, Hadronic molecules, *Rev. Mod. Phys.* **90**, 015004 (2018), [Erratum: Rev.Mod.Phys. 94, 029901 (2022)], arXiv:1705.00141 [hep-ph].
- [7] A. Ali, J. S. Lange, and S. Stone, Exotics: Heavy Pentaquarks and Tetraquarks, *Prog. Part. Nucl. Phys.* **97**, 123 (2017), arXiv:1706.00610 [hep-ph].

- [8] N. Brambilla, S. Eidelman, C. Hanhart, A. Nefediev, C.-P. Shen, C. E. Thomas, A. Vairo, and C.-Z. Yuan, The  $XYZ$  states: experimental and theoretical status and perspectives, *Phys. Rept.* **873**, 1 (2020), arXiv:1907.07583 [hep-ex].
- [9] Y.-R. Liu, H.-X. Chen, W. Chen, X. Liu, and S.-L. Zhu, Pentaquark and Tetraquark states, *Prog. Part. Nucl. Phys.* **107**, 237 (2019), arXiv:1903.11976 [hep-ph].
- [10] L. Meng, B. Wang, G.-J. Wang, and S.-L. Zhu, Chiral perturbation theory for heavy hadrons and chiral effective field theory for heavy hadronic molecules, *Phys. Rept.* **1019**, 1 (2023), arXiv:2204.08716 [hep-ph].
- [11] M. Mai, U.-G. Meißner, and C. Urbach, Towards a theory of hadron resonances, *Phys. Rept.* **1001**, 1 (2023), arXiv:2206.01477 [hep-ph].
- [12] H.-X. Chen, W. Chen, X. Liu, Y.-R. Liu, and S.-L. Zhu, An updated review of the new hadron states, *Rept. Prog. Phys.* **86**, 026201 (2023), arXiv:2204.02649 [hep-ph].
- [13] R. Aaij *et al.* (LHCb), Observation of structure in the  $J/\psi$ -pair mass spectrum, *Sci. Bull.* **65**, 1983 (2020), arXiv:2006.16957 [hep-ex].
- [14] A. Hayrapetyan *et al.* (CMS), New Structures in the  $J/\psi J/\psi$  Mass Spectrum in Proton-Proton Collisions at  $\sqrt{s}=13$  TeV, *Phys. Rev. Lett.* **132**, 111901 (2024), arXiv:2306.07164 [hep-ex].
- [15] G. Aad *et al.* (ATLAS), Observation of an Excess of Dicharmonium Events in the Four-Muon Final State with the ATLAS Detector, *Phys. Rev. Lett.* **131**, 151902 (2023), arXiv:2304.08962 [hep-ex].
- [16] C. Deng, H. Chen, and J. Ping, Towards the understanding of fully-heavy tetraquark states from various models, *Phys. Rev. D* **103**, 014001 (2021), arXiv:2003.05154 [hep-ph].
- [17] M.-S. Liu, F.-X. Liu, X.-H. Zhong, and Q. Zhao, Fully heavy tetraquark states and their evidences in LHC observations, *Phys. Rev. D* **109**, 076017 (2024), arXiv:2006.11952 [hep-ph].
- [18] X. Jin, Y. Xue, H. Huang, and J. Ping, Full-heavy tetraquarks in constituent quark models, *Eur. Phys. J. C* **80**, 1083 (2020), arXiv:2006.13745 [hep-ph].
- [19] Q.-F. Lü, D.-Y. Chen, and Y.-B. Dong, Masses of fully heavy tetraquarks  $QQ\bar{Q}\bar{Q}$  in an extended relativized quark model, *Eur. Phys. J. C* **80**, 871 (2020), arXiv:2006.14445 [hep-ph].
- [20] H.-X. Chen, W. Chen, X. Liu, and S.-L. Zhu, Strong decays of fully-charm tetraquarks into di-charmonia, *Sci. Bull.* **65**, 1994 (2020), arXiv:2006.16027 [hep-ph].
- [21] R. M. Albuquerque, S. Narison, A. Rabemananjara, D. Rabetiarivony, and G. Randriamanatrika, Doubly-hidden scalar heavy molecules and tetraquarks states from QCD at NLO, *Phys. Rev. D* **102**, 094001 (2020), arXiv:2008.01569 [hep-ph].
- [22] J. F. Giron and R. F. Lebed, Simple spectrum of  $c\bar{c}\bar{c}$  states in the dynamical diquark model, *Phys. Rev. D* **102**, 074003 (2020), arXiv:2008.01631 [hep-ph].
- [23] J.-Z. Wang, D.-Y. Chen, X. Liu, and T. Matsuki, Producing fully charm structures in the  $J/\psi$ -pair invariant mass spectrum, *Phys. Rev. D* **103**, 071503 (2021), arXiv:2008.07430 [hep-ph].
- [24] X.-K. Dong, V. Baru, F.-K. Guo, C. Hanhart, and A. Nefediev, Coupled-Channel Interpretation of the LHCb Double-  $J/\psi$  Spectrum and Hints of a New State Near the  $J/\psi J/\psi$  Threshold, *Phys. Rev. Lett.* **126**, 132001 (2021), [Erratum: *Phys.Rev.Lett.* 127, 119901 (2021)], arXiv:2009.07795 [hep-ph].
- [25] H.-F. Zhang and Y.-Q. Ma, Exploring the di- $J/\psi$  resonances based on  $\text{\it{itab}}$  initio perturbative QCD, (2020), arXiv:2009.08376 [hep-ph].
- [26] J. Zhao, S. Shi, and P. Zhuang, Fully-heavy tetraquarks in a strongly interacting medium, *Phys. Rev. D* **102**, 114001 (2020), arXiv:2009.10319 [hep-ph].
- [27] M. C. Gordillo, F. De Soto, and J. Segovia, Diffusion Monte Carlo calculations of fully-heavy multi-quark bound states, *Phys. Rev. D* **102**, 114007 (2020), arXiv:2009.11889 [hep-ph].
- [28] J.-R. Zhang,  $0^+$  fully-charmed tetraquark states, *Phys. Rev. D* **103**, 014018 (2021), arXiv:2010.07719 [hep-ph].
- [29] Z.-H. Guo and J. A. Oller, Insights into the inner structures of the fully charmed tetraquark state  $X(6900)$ , *Phys. Rev. D* **103**, 034024 (2021), arXiv:2011.00978 [hep-ph].
- [30] C. Gong, M.-C. Du, Q. Zhao, X.-H. Zhong, and B. Zhou, Nature of  $X(6900)$  and its production mechanism at LHCb, *Phys. Lett. B* **824**, 136794 (2022), arXiv:2011.11374 [hep-ph].
- [31] B.-D. Wan and C.-F. Qiao, Gluonic tetracharm configuration of  $X(6900)$ , *Phys. Lett. B* **817**, 136339 (2021), arXiv:2012.00454 [hep-ph].
- [32] H. G. Dosch, S. J. Brodsky, G. F. de Téramond, M. Nielsen, and L. Zou, Exotic states in a holographic theory, *Nucl. Part. Phys. Proc.* **312-317**, 135 (2021), arXiv:2012.02496 [hep-ph].
- [33] B.-C. Yang, L. Tang, and C.-F. Qiao, Scalar fully-heavy tetraquark states  $QQ'\bar{Q}\bar{Q}'$  in QCD sum rules, *Eur. Phys. J. C* **81**, 324 (2021), arXiv:2012.04463 [hep-ph].
- [34] Z. Zhao, K. Xu, A. Kaewsnod, X. Liu, A. Limphirat, and Y. Yan, Study of charmoniumlike and fully-charm tetraquark spectroscopy, *Phys. Rev. D* **103**, 116027 (2021), arXiv:2012.15554 [hep-ph].
- [35] R. N. Faustov, V. O. Galkin, and E. M. Savchenko, Heavy tetraquarks in the relativistic quark model, *Universe* **7**, 94 (2021), arXiv:2103.01763 [hep-ph].
- [36] H.-W. Ke, X. Han, X.-H. Liu, and Y.-L. Shi, Tetraquark state  $X(6900)$  and the interaction between diquark and antidiquark, *Eur. Phys. J. C* **81**, 427 (2021), arXiv:2103.13140 [hep-ph].
- [37] Z.-R. Liang, X.-Y. Wu, and D.-L. Yao, Hunting for states in the recent LHCb di- $J/\psi$  invariant mass spectrum, *Phys. Rev. D* **104**, 034034 (2021), arXiv:2104.08589 [hep-ph].
- [38] G. Yang, J. Ping, and J. Segovia, Exotic resonances of fully-heavy tetraquarks in a lattice-QCD inspired quark model, *Phys. Rev. D* **104**, 014006 (2021), arXiv:2104.08814 [hep-ph].
- [39] H. Mutuk, Nonrelativistic treatment of fully-heavy tetraquarks as diquark-antidiquark states, *Eur. Phys. J. C* **81**, 367 (2021), arXiv:2104.11823 [hep-ph].
- [40] Q. Li, C.-H. Chang, G.-L. Wang, and T. Wang, Mass spectra and wave functions of  $TQQ\bar{Q}$  tetraquarks, *Phys. Rev. D* **104**, 014018 (2021), arXiv:2104.12372 [hep-ph].
- [41] G.-J. Wang, L. Meng, M. Oka, and S.-L. Zhu, Higher fully charmed tetraquarks: Radial excitations and P-wave states, *Phys. Rev. D* **104**, 036016 (2021), arXiv:2105.13109 [hep-ph].
- [42] X.-K. Dong, V. Baru, F.-K. Guo, C. Hanhart, A. Nefediev, and B.-S. Zou, Is the existence of a  $J/\psi J/\psi$  bound state plausible?, *Sci. Bull.* **66**, 2462 (2021), arXiv:2107.03946 [hep-ph].
- [43] Q.-N. Wang, Z.-Y. Yang, and W. Chen, Exotic fully-heavy  $QQ\bar{Q}\bar{Q}$  tetraquark states in  $\mathbf{8}_{[Q\bar{Q}]} \otimes \mathbf{8}_{[Q\bar{Q}]}$  color configuration, *Phys. Rev. D* **104**, 114037 (2021), arXiv:2109.08091 [hep-ph].
- [44] F.-X. Liu, M.-S. Liu, X.-H. Zhong, and Q. Zhao, Higher mass spectra of the fully-charmed and fully-bottom tetraquarks, *Phys. Rev. D* **104**, 116029 (2021), arXiv:2110.09052 [hep-ph].
- [45] Z. Zhuang, Y. Zhang, Y. Ma, and Q. Wang, Lineshape of the compact fully heavy tetraquark, *Phys. Rev. D* **105**, 054026 (2022), arXiv:2111.14028 [hep-ph].
- [46] Z. Asadi and G. R. Boroun, Masses of fully heavy tetraquark states from a four-quark static potential model, *Phys. Rev. D* **105**, 014006 (2022), arXiv:2112.11028 [hep-ph].
- [47] C. Gong, M.-C. Du, and Q. Zhao, Pseudoscalar charmonium pair interactions via the Pomeron exchange mechanism, *Phys. Rev. D* **106**, 054011 (2022), arXiv:2206.13867 [hep-ph].
- [48] J.-Z. Wang and X. Liu, Improved understanding of the peaking



- phenomenon existing in the new di- $J/\psi$  invariant mass spectrum from the CMS Collaboration, *Phys. Rev. D* **106**, 054015 (2022), [arXiv:2207.04893 \[hep-ph\]](#).
- [49] Q. Zhou, D. Guo, S.-Q. Kuang, Q.-H. Yang, and L.-Y. Dai, Nature of the  $X(6900)$  in partial wave decomposition of  $J/\psi J/\psi$  scattering, *Phys. Rev. D* **106**, L111502 (2022), [arXiv:2207.07537 \[hep-ph\]](#).
- [50] G.-J. Wang, Q. Meng, and M. Oka, S-wave fully charmed tetraquark resonant states, *Phys. Rev. D* **106**, 096005 (2022), [arXiv:2208.07292 \[hep-ph\]](#).
- [51] P.-Y. Niu, E. Wang, Q. Wang, and S. Yang, Determine the quantum numbers of  $X(6900)$  from photon-photon fusion in ultra-peripheral heavy ion collisions, (2022), [arXiv:2209.01924 \[hep-ph\]](#).
- [52] W.-C. Dong and Z.-G. Wang, Going in quest of potential tetraquark interpretations for the newly observed  $T\psi\psi$  states in light of the diquark-antidiquark scenarios, *Phys. Rev. D* **107**, 074010 (2023), [arXiv:2211.11989 \[hep-ph\]](#).
- [53] G.-L. Yu, Z.-Y. Li, Z.-G. Wang, J. Lu, and M. Yan, The S- and P-wave fully charmed tetraquark states and their radial excitations, *Eur. Phys. J. C* **83**, 416 (2023), [arXiv:2212.14339 \[hep-ph\]](#).
- [54] P. G. Ortega, D. R. Entem, and F. Fernández, Exploring  $T\psi\psi$  tetraquark candidates in a coupled-channels formalism, *Phys. Rev. D* **108**, 094023 (2023), [arXiv:2307.00532 \[hep-ph\]](#).
- [55] G.-J. Wang, M. Oka, and D. Jido, Quark confinement for multi-quark systems: Application to fully charmed tetraquarks, *Phys. Rev. D* **108**, L071501 (2023).
- [56] W.-L. Sang, T. Wang, Y.-D. Zhang, and F. Feng, Electromagnetic and hadronic decay of fully heavy tetraquark, (2023), [arXiv:2307.16150 \[hep-ph\]](#).
- [57] M. N. Anwar and T. J. Burns, Structure of  $cc\bar{c}\bar{c}$  tetraquarks and interpretation of LHC states, (2023), [arXiv:2311.15853 \[hep-ph\]](#).
- [58] Y. Wu, X. Liu, Y. Tan, H. Huang, and J. Ping, Further study of  $c\bar{c}c\bar{c}$  system within a chiral quark model, (2024), [arXiv:2403.10375 \[hep-ph\]](#).
- [59] W. Chen, H.-X. Chen, X. Liu, T. G. Steele, and S.-L. Zhu, Hunting for exotic doubly hidden-charm/bottom tetraquark states, *Phys. Lett. B* **773**, 247 (2017), [arXiv:1605.01647 \[hep-ph\]](#).
- [60] Z.-Z. Chen, X.-L. Chen, P.-F. Yang, and W. Chen, P-wave fully charm and fully bottom tetraquark states, *Phys. Rev. D* **109**, 094011 (2024), [arXiv:2402.03117 \[hep-ph\]](#).
- [61] V. R. Debastiani and F. S. Navarra, A non-relativistic model for the  $[cc][\bar{c}\bar{c}]$  tetraquark, *Chin. Phys. C* **43**, 013105 (2019), [arXiv:1706.07553 \[hep-ph\]](#).
- [62] M. A. Bedolla, J. Ferretti, C. D. Roberts, and E. Santopinto, Spectrum of fully-heavy tetraquarks from a diquark+antidiquark perspective, *Eur. Phys. J. C* **80**, 1004 (2020), [arXiv:1911.00960 \[hep-ph\]](#).
- [63] E. Hiyama, Y. Kino, and M. Kamimura, Gaussian expansion method for few-body systems, *Progress in Particle and Nuclear Physics* **51**, 223 (2003).
- [64] J. Aguilar and J. M. Combes, A class of analytic perturbations for one-body schroedinger hamiltonians, *Commun. Math. Phys.* **22**, 269 (1971).
- [65] E. Balslev and J. M. Combes, Spectral properties of many-body schroedinger operators with dilatation-analytic interactions, *Commun. Math. Phys.* **22**, 280 (1971).
- [66] S. Aoyama, T. Myo, K. Katō, and K. Ikeda, The complex scaling method for many-body resonances and its applications to three-body resonances, *Progress of theoretical physics* **116**, 1 (2006).
- [67] L. Meng, Y.-K. Chen, Y. Ma, and S.-L. Zhu, Tetraquark bound states in constituent quark models: Benchmark test calculations, *Phys. Rev. D* **108**, 114016 (2023), [arXiv:2310.13354 \[hep-ph\]](#).
- [68] Y.-K. Chen, W.-L. Wu, L. Meng, and S.-L. Zhu, Unified description of the  $Qsq\bar{q}$  molecular bound states, molecular resonances, and compact tetraquark states in the quark potential model, *Phys. Rev. D* **109**, 014010 (2024), [arXiv:2310.14597 \[hep-ph\]](#).
- [69] W.-L. Wu, Y. Ma, Y.-K. Chen, L. Meng, and S.-L. Zhu, Fully heavy tetraquark resonant states with different flavors, *Phys. Rev. D* **110**, 034030 (2024), [arXiv:2406.17824 \[hep-ph\]](#).
- [70] W.-L. Wu, Y. Ma, Y.-K. Chen, L. Meng, and S.-L. Zhu, Doubly heavy tetraquark bound and resonant states, *Phys. Rev. D* **110**, 094041 (2024), [arXiv:2409.03373 \[hep-ph\]](#).
- [71] T. Barnes, S. Godfrey, and E. S. Swanson, Higher charmonia, *Phys. Rev. D* **72**, 054026 (2005), [arXiv:hep-ph/0505002](#).
- [72] S. Navas *et al.* (Particle Data Group), Review of particle physics, *Phys. Rev. D* **110**, 030001 (2024).
- [73] Y. Ma, W.-L. Wu, L. Meng, Y.-K. Chen, and S.-L. Zhu, Fully strange tetraquark resonant states as the cousins of  $X(6900)$ , *Phys. Rev. D* **110**, 074026 (2024), [arXiv:2408.00503 \[hep-ph\]](#).